An augmented Lagrangian coordination method for distributed optimal design in MDO: Part II examples

Systems Engineering Group
Department of Mechanical Engineering
Eindhoven University of Technology
PO Box 513
5600 MB Eindhoven
The Netherlands
http://se.wtb.tue.nl/

SE Report: Nr. 2007-05

An augmented Lagrangian coordination method for distributed optimal design in MDO: Part II examples

S. Tosserams, L.F.P. Etman, and J.E. Rooda

ISSN: 1872-1567

SE Report: Nr. 2007-05
Eindhoven, February 2007
SE Reports are available via http://se.wtb.tue.nl/sereports

Abstract

The formulation flexibility and the numerical performance of the augmented Lagrangian coordination method proposed in the part I paper is demonstrated on several example problems. Results for a number of test problems indicate that the coordination method is effective and robust in finding solutions of the original non-decomposed problem, and does not introduce new local minima for non-convex problems. The required coordination costs are found to be determined by how the problem is partitioned and coordinated. These costs do not only depend on the number of quantities that have to be coordinated, but also on their coupling strengths. The formulation flexibility of the new method provides means to minimize these costs by adapting the problem at hand.

1 Introduction

In Part I [1] of this study, an augmented Lagrangian coordination method is described for multidisciplinary design optimization (MDO) problem with coupling variables and coupling functions. Two formulation variants are proposed, offering the designer a large degree of freedom in tailoring the coordination method to the specific requirements of the design problem. Presented solution algorithms can be shown to converge to Karush-Kuhn-Tucker (KKT) points of the original non-decomposed problem. The purpose of this study is to demonstrate the flexibility offered by the formulation, and to investigate its numerical behavior on a number of test problems. For details of the coordination method, the reader is referred to Part I [1].

Section 2 demonstrates the flexibility offered by the formulation variants on a geometric programming problem. For this example, Section 3 discusses numerical performance of the coordination algorithm under different inner loop termination strategies. Numerical performance on the portal frame problem – a non-convex structural optimization problem with multiple local minima – is discussed in Section 4. Section 5 presents results on a conceptual level aircraft design problem. With this example, we investigate the performance of the method when the solutions to the original problems are not KKT points, and hence do not satisfy the assumptions for the convergence proof of the coordination algorithms. Section 6 gives a concluding discussion on the performance of the coordination method, and suggests possible improvements.

2 Geometric programming problem: Formulation flexibility

The first example is a geometric programming problem with 14 variables, 4 inequality constraints, and 3 equality constraints. This example is used to demonstrate the formulation flexibility offered by the augmented Lagrangian coordination method.

The all-in-one geometric programming problem is given by:

$$
\begin{aligned}
\min_{z_1,\ldots,z_{14}} \quad & f = F_1 + F_2 = 0.1 z_1^2 z_2^2 z_7^2 + z_8^{-2} z_{11}^2 z_7^2 \\
\text{subject to} \quad & g_1 = (z_3^{-2} + z_4^2) z_5^{-2} - 1 \leq 0 \\
& g_2 = (z_8^2 + z_9^2) z_{11}^{-2} - 1 \leq 0 \\
& g_3 = (z_{11}^2 + z_{12}^{-2}) z_{13}^{-2} - 1 \leq 0 \\
& g_4 = (z_5^2 + z_6^{-2}) z_7^{-2} + (z_8^{-2} + z_{10}^2) z_{11}^{-2} + (z_{11}^2 + z_{12}^2) z_{14}^{-2} - 3 \leq 0 \\
& h_1 = (z_3^2 + z_4^{-2} + z_5^2) z_1^{-2} - 1 = 0 \\
& h_2 = (z_{11}^2 + z_{12}^2 + z_{13}^2 + z_{14}^2) z_6^{-2} - 1 = 0 \\
& h_3 = (z_5^2 + z_6^2 + z_7^2) z_2^{-2} + (z_8^2 + z_9^{-2} + z_{10}^{-2} + z_{11}^2) z_3^{-2} - 2 = 0 \\
& 0.1 \leq z_1, z_2, \ldots, z_{14} \leq 10
\end{aligned}
\tag{1}
$$

The unique optimal solution to this problem, obtained with Matlab 7.1's SQP solver `fmincon` [2] is (rounded): $\mathbf{z}^* = [5.3660, 2.7879, 4.1147, 0.2921, 0.3800, 3.4117, 0.3407, 1.2098, 0.7400, 0.6157, 1.4182, 0.7567, 1.9385, 2.3017]$, with $f(\mathbf{z}^*) = 2.7572$.

2.1 Decomposed formulation variants

To demonstrate the two formulation variants, the problem is partitioned into three subsystems. Subsystem 1 has local variables $\mathbf{x}_1 = [z_1, z_2, z_3, z_4, z_5]$, no local objective $f_1 = 0$, and local constraints $\mathbf{g}_1 = [g_1]$ and $\mathbf{h}_1 = [h_1]$. Subsystem 2 has local variables $\mathbf{x}_2 = [z_7, z_8, z_9, z_{10}]$, local objec-

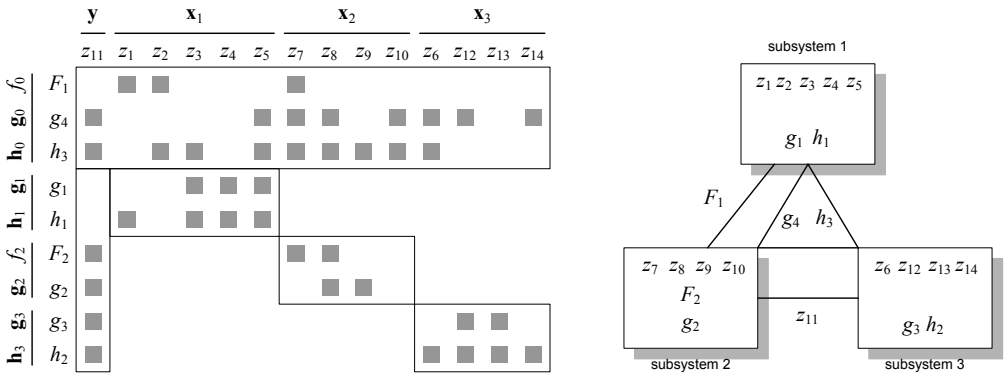

(a) Functional dependence table for partitioned geometric optimization problem

(b) Illustration of partition structure

Figure 1: Example 1: Partition structure

tive $f_2 = F_2$, and local constraints $\mathbf{g}_2 = [g_2]$ and $\mathbf{h}_2 = []$. Subsystem 3 has $\mathbf{x}_3 = [z_6, z_{12}, z_{13}, z_{14}]$, $f_3 = 0$, and $\mathbf{g}_3 = [g_3]$ and $\mathbf{h}_3 = [h_2]$. All subsystems are coupled through coupling constraints $\mathbf{g}_0 = [g_4]$ and $\mathbf{h}_0 = [h_3]$. Subsystems 1 and 2 are coupled through the coupling objective $f_0 = F_1$, and subsystems 2 and 3 are linked through coupling variable $\mathbf{y} = [z_{11}]$, which gives $\mathbf{y}_1 = []$, $\mathbf{y}_2 = [z_{11,2}]$, $\mathbf{y}_3 = [z_{11,3}]$, where the second index refers to the subsystem of computation. The functional dependence table (FDT) for problem (1) is given in Fig. 1(a), in which the selected partition is indicated. The problem structure associated with the above partition is depicted in Fig. 1(b).

Centralized formulation

A centralized formulation is used to demonstrate how the partition can be coordinated in a classic multi-disciplinary fashion. For the centralized formulation variant, a master problem is introduced to solve for the master copy of shared variables $\mathbf{y} = [z_{11}]$, as well as for the slack variable x_0 introduced by relaxing the coupling inequality constraint $\mathbf{g}_0 = [g_4]$. Since only subsystems 2 and 3 depend on the shared variables, we have for the selection matrices: $\mathbf{S}_1 = []$, $\mathbf{S}_2 = [1]$, and $\mathbf{S}_3 = [1]$, which yields the consistency constraints: $c_2 = z_{11} - z_{11,2} = 0$ and $c_3 = z_{11} - z_{11,3} = 0$.

The master problem P_0 for the centralized formulation is given by:

$$
\begin{aligned}
\min_{z_{11},x_0} \quad & z_8^{-2} z_{11}^2 z_7^2 + v_{c,2}(z_{11} - z_{11,2}) + w_{c,2}^2 (z_{11} - z_{11,2})^2 + v_{c,3}(z_{11} - z_{11,3}) + w_{c,3}^2 (z_{11} - z_{11,3})^2 \\
& + v_g(g_4 + x_0^2) + w_g^2 (g_4 + x_0^2)^2 + v_h h_3 + w_h^2 h_3^2 \\
\text{subject to} \quad & 0.1 \le z_{11} \le 10 \\
\text{where} \quad & g_4 = (z_5^2 + z_6^{-2}) z_7^{-2} + (z_8^{-2} + z_{10}^2) z_{11}^{-2} + (z_{11}^2 + z_{12}^2) z_{14}^{-2} - 3 \\
& h_3 = (z_5^2 + z_6^2 + z_7^2) z_2^{-2} + (z_8^2 + z_9^{-2} + z_{10}^{-2} + z_{11}^2) z_3^{-2} - 2
\end{aligned}
\tag{2}
$$

where the objective is the sum of the coupling objective (first term), consistency penalties (second to fifth term), and coupling constraints penalties (sixth to ninth term).

3 Geometric programming problem: Formulation flexibility

Subproblem P_1 associated with subsystem 1 is given by:

$$\begin{aligned}
\min_{z_1,z_2,z_3,z_4,z_5} \quad & 0.1z_1^2z_2^2z_7^2 + v_g(g_4+x_0^2) + w_g^2(g_4+x_0^2)^2 + v_h h_3 + w_h^2 h_3^2 \\
\text{subject to} \quad & g_1 = (z_3^{-2}+z_4^2)z_5^{-2} - 1 \le 0 \\
& h_1 = (z_3^2+z_4^{-2}+z_5^2)z_1^{-2} - 1 = 0 \\
& 0.1 \le z_1,z_2,z_3,z_4,z_5 \le 10 \\
\text{where} \quad & g_4 = (z_5^2+z_6^{-2})z_7^{-2} + (z_8^{-2}+z_{10}^2)z_{11}^{-2} + (z_{11}^2+z_{12}^2)z_{14}^{-2} - 3 \\
& h_3 = (z_5^2+z_6^2+z_7^2)z_2^{-2} + (z_8^2+z_9^{-2}+z_{10}^{-2}+z_{11}^2)z_3^{-2} - 2
\end{aligned} \tag{3}$$

which includes only the coupling objective (first term), and the coupling constraint penalties (second to fifth term).

Similarly, subproblem P_2 associated with subsystem 2 is given by:

$$\begin{aligned}
\min_{z_7,z_8,z_9,z_{10},z_{11,2}} \quad & 0.1z_1^2z_2^2z_7^2 + z_8^{-2}z_{11,2}^2z_7^2 + v_{c,2}(z_{11}-z_{11,2}) + w_{c,2}^2(z_{11}-z_{11,2})^2 \\
& + v_g(g_4+x_0^2) + w_g^2(g_4+x_0^2)^2 + v_h h_3 + w_h^2 h_3^2 \\
\text{subject to} \quad & g_2 = (z_8^2+z_9^2)z_{11,2}^{-2} - 1 \le 0 \\
& 0.1 \le z_7,z_8,z_9,z_{10},z_{11,2} \le 10 \\
\text{where} \quad & g_4 = (z_5^2+z_6^{-2})z_7^{-2} + (z_8^{-2}+z_{10}^2)z_{11}^{-2} + (z_{11}^2+z_{12}^2)z_{14}^{-2} - 3 \\
& h_3 = (z_5^2+z_6^2+z_7^2)z_2^{-2} + (z_8^2+z_9^{-2}+z_{10}^{-2}+z_{11}^2)z_3^{-2} - 2
\end{aligned} \tag{4}$$

where besides the coupling objective (first term), a local objective is included (second term) as well as the consistency penalty on $z_{11,2}$ (third and fourth term), and the coupling constraint penalty (fifth to eighth term),

Subproblem P_3 associated with subsystem 3 is given by:

$$\begin{aligned}
\min_{z_6,z_{11,3},z_{12},z_{13},z_{14}} \quad & v_{c,3}(z_{11}-z_{11,3}) + w_{c,3}^2(z_{11}-z_{11,3})^2 \\
& + v_g(g_4+x_0^2) + w_g^2(g_4+x_0^2)^2 + v_h h_3 + w_h^2 h_3^2 \\
\text{subject to} \quad & g_3 = (z_{11,3}^2+z_{12}^{-2})z_{13}^{-2} - 1 \le 0 \\
& h_2 = (z_{11,3}^2+z_{12}^2+z_{13}^2+z_{14}^2)z_6^{-2} - 1 = 0 \\
& 0.1 \le z_6,z_{11,3},z_{12},z_{13},z_{14} \le 10 \\
\text{where} \quad & g_4 = (z_5^2+z_6^{-2})z_7^{-2} + (z_8^{-2}+z_{10}^2)z_{11}^{-2} + (z_{11}^2+z_{12}^2)z_{14}^{-2} - 3 \\
& h_3 = (z_5^2+z_6^2+z_7^2)z_2^{-2} + (z_8^2+z_9^{-2}+z_{10}^{-2}+z_{11}^2)z_3^{-2} - 2
\end{aligned} \tag{5}$$

which only includes a penalty on the consistency of $z_{11,3}$ (first and second term), and the penalties on the coupling constraints (third to sixth term).

The structure of the centralized formulation is illustrated in Fig. 2. The lines between subproblems indicate coupling through the coupling objective and the penalty terms on the coupling constraints (dashed lines), and coupling through the penalty terms on the consistency constraints (solid lines).

Distributed formulation

For the distributed formulation variant, we coordinate coupling between subsystems without the use of a master problem. Instead, the coupling is coordinated directly between subsystems. If, for example, subsystem 1 is a system-level design problem, it can be superimposed over the subsystems 2 and 3. In that case, subsystem 1 may be selected to also include the task of solving for x_0, which was allocated to the master problem P_0 in the centralized formulation. Furthermore, we can choose to coordinate coupling through z_{11} directly between subsystems 2 and 3 by setting the selection matrices $\mathbf{S}_{23} = \mathbf{S}_{32} = [1]$ and defining the neighbors as $\mathcal{N}_1 = \{\}$, $\mathcal{N}_2 = \{3\}$, and $\mathcal{N}_3 = \{2\}$, which yields $c_{23} = z_{11,2} - z_{11,3} = 0$. Subsystem 3 can be assigned to solve for the shared variable z_{11} in the coupling constraints by setting $\mathbf{T}_1 = \mathbf{T}_2 = []$ and $\mathbf{T}_3 = [1]$.

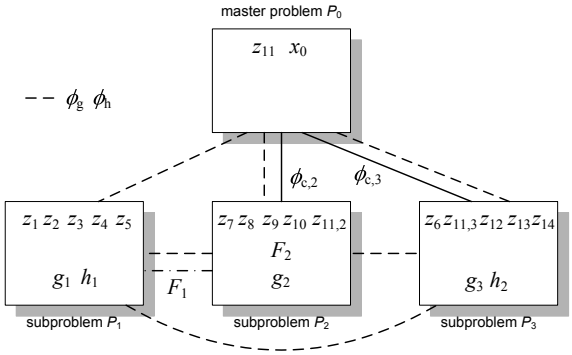

Figure 2: Example 1: Centralized formulation structure

Under these choices, subproblem P_1 in the distributed formulation is given by:

$$\begin{array}{rl} \min\limits_{z_1,z_2,z_3,z_4,z_5,x_0} & 0.1z_1^2z_2^2z_7^2 + v_g(g_4+x_0^2) + w_g^2(g_4+x_0^2)^2 + v_h h_3 + w_h^2 h_3^2 \\ \text{subject to} & g_1 = (z_3^{-2}+z_4^2)z_5^{-2} - 1 \le 0 \\ & h_1 = (z_3^2+z_4^{-2}+z_5^2)z_1^{-2} - 1 = 0 \\ & 0.1 \le z_1, z_2, z_3, z_4, z_5 \le 10 \\ \text{where} & g_4 = (z_5^2+z_6^{-2})z_7^{-2} + (z_8^{-2}+z_{10}^2)z_{11,3}^{-2} + (z_{11,3}^2+z_{12}^2)z_{14}^{-2} - 3 \\ & h_3 = (z_5^2+z_6^2+z_7^2)z_2^{-2} + (z_8^2+z_9^{-2}+z_{10}^{-2}+z_{11,3}^2)z_3^{-2} - 2 \end{array} \tag{6}$$

Subproblem P_2 associated with subsystem 2 is given by:

$$\begin{array}{rl} \min\limits_{z_7,z_8,z_9,z_{10},z_{11,2}} & 0.1z_1^2z_2^2z_7^2 + z_8^{-2}z_{11,2}^2z_7^2 + v_{c,23}(z_{11,2}-z_{11,3}) + w_{c,23}^2(z_{11,2}-z_{11,3})^2 \\ & + v_g(g_4+x_0^2) + w_g^2(g_4+x_0^2)^2 + v_h h_3 + w_h^2 h_3^2 \\ \text{subject to} & g_2 = (z_8^2+z_9^2)z_{11,2}^{-2} - 1 \le 0 \\ & 0.1 \le z_7, z_8, z_9, z_{10}, z_{11,2} \le 10 \\ \text{where} & g_4 = (z_5^2+z_6^{-2})z_7^{-2} + (z_8^{-2}+z_{10}^2)z_{11,3}^{-2} + (z_{11,3}^2+z_{12}^2)z_{14}^{-2} - 3 \\ & h_3 = (z_5^2+z_6^2+z_7^2)z_2^{-2} + (z_8^2+z_9^{-2}+z_{10}^{-2}+z_{11,3}^2)z_3^{-2} - 2 \end{array} \tag{7}$$

Subproblem P_3 associated with subsystem 3 is given by:

$$\begin{array}{rl} \min\limits_{z_6,z_{11,3},z_{12},z_{13},z_{14}} & v_{c,23}(z_{11,2}-z_{11,3}) + w_{c,23}^2(z_{11,2}-z_{11,3})^2 \\ & + v_g(g_4+x_0^2) + w_g^2(g_4+x_0^2)^2 + v_h h_3 + w_h^2 h_3^2 \\ \text{subject to} & g_3 = (z_{11,3}^2+z_{12}^{-2})z_{13}^{-2} - 1 \le 0 \\ & h_2 = (z_{11,3}^2+z_{12}^2+z_{13}^2+z_{14}^2)z_6^{-2} - 1 = 0 \\ & 0.1 \le z_6, z_{11,3}, z_{12}, z_{13}, z_{14} \le 10 \\ \text{where} & g_4 = (z_5^2+z_6^{-2})z_7^{-2} + (z_8^{-2}+z_{10}^2)z_{11,3}^{-2} + (z_{11,3}^2+z_{12}^2)z_{14}^{-2} - 3 \\ & h_3 = (z_5^2+z_6^2+z_7^2)z_2^{-2} + (z_8^2+z_9^{-2}+z_{10}^{-2}+z_{11,3}^2)z_3^{-2} - 2 \end{array} \tag{8}$$

The structure of the distributed formulation is depicted in Fig. 3. The lines between subproblems indicate coupling through the coupling objective and coupling constraint penalties (dashed lines), and coupling through the consistency penalty terms (solid lines).

Other distributed formulations can be defined by choosing different selection matrices $\mathbf{T}_j$ and consistency constraints, offering the designer a large degree of flexibility in setting up a coordination strategy.

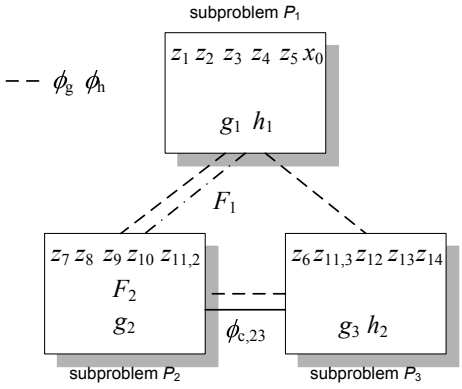

Figure 3: Example 1: Distributed formulation structure

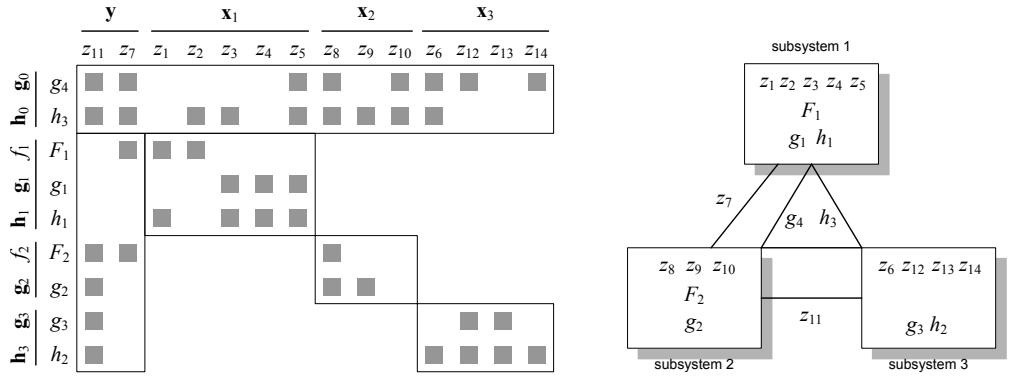

(a) Functional dependence table for partitioned geometric optimization problem

(b) Illustration of partition structure

Figure 4: Example 1: Partition structure with z_7 as coupling variable and F_1 as local objective to subsystem 1

2.2 Coupling function versus coupling variable

The augmented Lagrangian coordination method also offers flexibility in deciding whether coupling between two subproblems is coordinated as a coupling function or a (set of) coupling variables. In the previous two formulations of the geometric programming problem, we selected F_1 as a coupling function that links subsystems 1 and 2. Instead, we could also opt for adding z_7 to the set of coupling variables $\mathbf{y} = [z_7, z_{11}]$. By treating z_7 as a coupling variable, objective F_1 can be treated as an objective function local to subsystem 1. The objective function F_1 is now purely local to subsystem 1 at the expense of coupling through z_7. The problem structure for this alternative partition is given in Fig. 4. Which choice of partition is preferred typically depends on the problem at hand.

The above formulation examples show that the proposed augmented Lagrangian coordination method provides a large degree of freedom in setting up a coordination scheme suited to a specific problem. The two formulation variants offer freedom in the overall information flows, and the distinction between coupling functions and coupling variables supplies flexibility in treating functions and variables either local or as a coordinated quantity.

3 Geometric programming problem: Numerical performance

In this section, the numerical performance of the solution algorithms of the augmented Lagrangian coordination method is investigated. Both the exact and the inexact solution algorithms from Ref. [1] are used to solve the partitioned problems of the geometric programming problem of Section 2.

First, we investigate the performance differences between the two formulation variants (centralized and distributed) of Section 2.1. Second, the implications of using either a coupling objective or a coupling variable are illustrated for the example of Section 2.2. Third, we introduce a third partition of the geometric programming problem to assess the influence of the amount of interaction between subsystems on numerical performance.

3.1 Experiments setup

For each partitioned problem, two algorithmic parameters are varied to investigate the numerical performance of the coordination method: the outer loop termination tolerance ε and the initial starting point $\mathbf{z}^0$. Four outer loop termination tolerances are selected: $\varepsilon = 10^{-2}, 10^{-3}, 10^{-4}, 10^{-5}$. For each decomposed problem, five initial designs $\mathbf{z}_i^0$, $i = 1,\ldots,5$, with components selected randomly between 0 and 5 are used (Table 1). Performance results are then taken as the average over these five initial designs.

	Initial design													
i	z_1	z_2	z_3	z_4	z_5	z_6	z_7	z_8	z_9	z_{10}	z_{11}	z_{12}	z_{13}	z_{14}
1	3.3638	0.4771	0.0868	4.1100	3.0106	0.8515	4.3842	4.6334	1.1358	2.5460	3.8544	4.7385	4.5413	3.2582
2	4.7900	0.0743	4.0970	1.3161	3.0247	2.6980	0.0645	3.3936	2.5813	0.3714	1.5696	4.1401	0.7819	3.7701
3	3.8328	1.4410	3.1057	3.7682	3.2975	3.1170	1.5520	0.3716	2.2910	0.9662	3.1910	4.5878	0.6106	3.3158
4	3.3306	4.0837	2.8011	3.2982	0.9168	3.4294	3.8954	0.3533	3.5160	1.8980	4.9328	0.5654	3.8133	4.4175
5	0.6547	4.9274	1.2202	1.0703	3.1827	3.3867	1.5365	0.0597	2.9124	1.3822	2.5144	4.0606	3.6090	1.3608

Table 1: Initial designs for geometric programming problem (1)

Problems are solved with both the exact and inexact method of multipliers solution algorithms (EM and IM, respectively). For EM, we take the inner loop termination tolerance equal to $\varepsilon_{\text{inner}} = 0.01\varepsilon$. For IM, we decrease the inner loop termination tolerance from 1 initially to 0.01ε in 10 outer loop steps, after which the inner loop tolerance remains equal to 0.01ε. The inner loop termination tolerance $\varepsilon_{\text{inner}}^k$ for the kth outer loop iteration is given by:

$$\varepsilon_{\text{inner}}^k = \max(0.01\varepsilon, 10^{\frac{k}{10}\log(0.01\varepsilon)}) \tag{9}$$

Optimization problems are solved with Matlab's SQP algorithm `fmincon` [2] where the tolerances `TolX`, `TolFun`, and `TolCon` are taken equal to $0.01\varepsilon_{\text{inner}}^{(k)}$, and gradients are computed through the built-in finite difference routine of `fmincon`.

For each termination tolerance, we determine the required number of subproblem optimizations and the final solution error, both taken as the average over the five initial designs. The number of subproblem optimizations can be seen as a measure for the costs associated with coordinating the solution of the decomposed problem. The solution error, defined as:

$$e = \frac{|f^* - f^K|}{1 + |f^*|} \tag{10}$$

is a measure for the accuracy of the solution. In Eq. (10), $f^* = f(\mathbf{z}^*)$ is the minimum of the original objective function, as obtained from the AIO problem, $f^K = f(\mathbf{z}^K)$ is the objective function

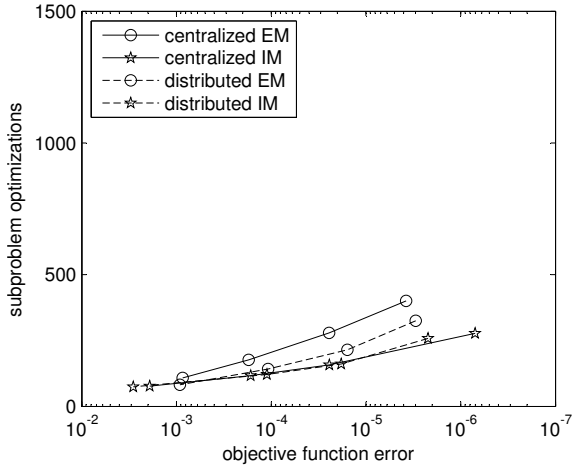

Figure 5: Example 1, Partition 1: Numerical results for centralized (solid lines) and distributed formulation (dashed lines), and exact (EM, ∘) and inexact (IM, ⋆) inner loop solution algorithms for different termination tolerances

value at the solution $\mathbf{z}^K$ obtained at convergence of the coordination algorithm[1]. The division by $1+|f^*|$ is used for appropriate scaling for large as well as small values of the objective function.

3.2 Centralized versus distributed formulation

Figure 5 depicts the results for the decomposed problem of Section 2.1 in the centralized formulation (solid lines) and the distributed formulation (dashed lines). The results for the exact inner loop EM are indicated with circle markers, and star markers are used for the inexact inner loop IM. A marker on each line is associated with a specific tolerance $\varepsilon = 10^{-2}$, 10^{-3}, 10^{-4}, or 10^{-5} (markers from left to right). Throughout this section, identical axis ranges are used to allow easy comparison of results.

The results in Figure 5 suggest that the distributed formulation (dashed lines) requires an equal number or less subproblem optimizations when compared to the centralized formulation (solid lines). Similar behavior is observed for other test problems indicating that a distributed formulation is at least as efficient as the centralized formulation, and often more efficient. An explanation for this may be that the number of consistency constraints, to which coordination effort is proportional, is smaller for the distributed formulation. In the distributed formulation of this example, only 1 consistency constraint is present (c_{23}), whereas for the centralized formulation 2 consistency constraints (c_2 and c_3) are used.

The figure also shows that the inexact inner loop (IM, stars) requires a lower number of subproblem optimizations than the exact inner loop (EM, circles). Reductions become larger for more accurate solutions, and can go up to 25-50% for an error of 10^{-5}. As expected, a computational advantage is gained by solving the first number of inner loop problems to a lower accuracy.

[1]For the centralized formulation, the components of $\mathbf{z}^K$ associated with the shared variables are takes as the average of all local copies $\mathbf{y}_j,\ j=1,\ldots,M$ and the master copy $\mathbf{y}$. In case of the distributed formulation, the average is taken only with respect to the local copies $\mathbf{y}_j,\ j=1,\ldots,M$ since no master level copy exists.

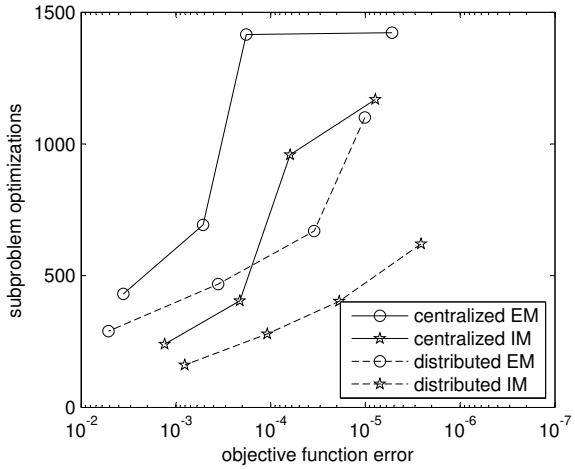

Figure 6: Example 1, Partition 2: Numerical results for centralized (solid lines) and distributed formulation (dashed lines), and exact (EM, ○) and inexact (IM, ⋆) inner loop solution algorithms for different termination tolerances

3.3 Coupling objective versus coupling variable

Figure 6 depicts the results for Partition 2, as described in Section 2. In this partition, z_7 is treated as a coupling variable and F_1 is local to subsystem 1. Solid lines correspond to a centralized formulation, and dashed lines are associated with the distributed formulation. Markers correspond to the termination tolerances $\varepsilon = 10^{-2}, 10^{-3}, 10^{-4}, 10^{-5}$ (left to right).

A difference between the results for this partition, and Partition 1 (Fig. 5) can clearly be observed. Partition 1 with the coupling objective requires a factor 2-5 less subproblem optimizations when compared to Partition 2 with the coupling variable. This difference is observed for both the centralized and the distributed formulation. An explanation for these differences is the fact that a coupling objective does not require penalty parameters to be set in the outer loop where a coupling variable does. A coupling through the objective of Partition 1 can be resolved in a single outer loop iteration, but the consistency constraint on z_7 of Partition 2 requires a number of outer loop iterations to find the optimal values for the penalty parameters. The increased number of outer loop iterations for Partition 2 is expected to cause the difference in computational costs between the two partitions.

3.4 Three-level partition

To investigate the effect of an increased amount of coupling, a third partition of the geometric programming problem is introduced. This more strongly coupled partition consists of five subsystems coupled through the variables $\mathbf{y} = [z_1, z_2, z_3, z_5, z_6, z_{11}]$, objective function $f_0 = F_1 + F_2$, and constraints $\mathbf{g}_0 = [g_4]$ and $\mathbf{h}_0 = [h_3]$. The local variables for each subsystem are: $\mathbf{x}_1 = []$, $\mathbf{x}_2 = [z_4]$, $\mathbf{x}_3 = [z_7]$, $\mathbf{x}_4 = [z_8, z_9, z_{10}]$, and $\mathbf{x}_5 = [z_{12}, z_{13}, z_{14}]$. Subsystems do not have local objectives $f_1 = f_2 = f_3 = f_4 = f_5 = 0$, and only subsystems 2, 4, and 5 have local constraints: $\mathbf{g}_1 = \mathbf{g}_3 = []$, $\mathbf{g}_2 = [g_1]$, $\mathbf{g}_4 = [g_2]$, $\mathbf{g}_5 = [g_3]$, $\mathbf{h}_1 = \mathbf{h}_3 = \mathbf{h}_4 = []$, $\mathbf{h}_2 = [h_1]$, $\mathbf{h}_5 = [h_2]$. The problem structure for Partition 3 is depicted in Figure 7. The selection matrices for the distributed formulation are as given in Table 2.

The exact (EM) and inexact (IM) coordination algorithms are used to solve this partition in both the centralized (solid lines) and distributed formulation (dashed lines). Figure 8 shows the results of the third partition for $\varepsilon = 10^{-2}, 10^{-3}, 10^{-4}$, or 10^{-5} (markers from left to right).

subsystem 1	subsystem 2	subsystem 3	subsystem 4	subsystem 5
$\mathcal{N}_1 = \{2,3\}$	$\mathcal{N}_2 = \{1,3,4\}$	$\mathcal{N}_3 = \{1,2,5\}$	$\mathcal{N}_4 = \{2,5\}$	$\mathcal{N}_5 = \{3,4\}$
	$\mathbf{S}_{21} = [1\ 0\ 0]$	$\mathbf{S}_{31} = [1\ 0\ 0]$	$\mathbf{S}_{41} = []$	$\mathbf{S}_{51} = []$
$\mathbf{S}_{12} = [1\ 0]$		$\mathbf{S}_{32} = [0\ 1\ 0]$	$\mathbf{S}_{42} = [1\ 0]$	$\mathbf{S}_{52} = []$
$\mathbf{S}_{13} = [0\ 1]$	$\mathbf{S}_{23} = [0\ 0\ 1]$		$\mathbf{S}_{43} = []$	$\mathbf{S}_{53} = [1\ 0]$
$\mathbf{S}_{14} = []$	$\mathbf{S}_{24} = [0\ 1\ 0]$	$\mathbf{S}_{34} = []$		$\mathbf{S}_{54} = [0\ 1]$
$\mathbf{S}_{15} = []$	$\mathbf{S}_{25} = []$	$\mathbf{S}_{35} = [0\ 0\ 1]$	$\mathbf{S}_{45} = [0\ 1]$	
$\mathbf{T}_1 = [1\ 0; 0\ 1]$	$\mathbf{T}_2 = [0\ 0\ 1]$	$\mathbf{T}_3 = [0\ 0\ 1]$	$\mathbf{T}_4 = [1\ 0]$	$\mathbf{T}_5 = [0\ 1]$

Table 2: Selection matrices for Partition 3

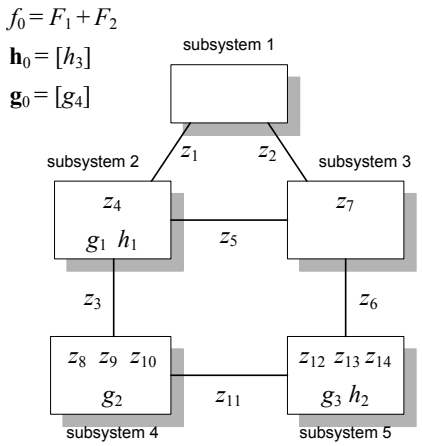

Figure 7: Example 1: Partition 3 problem structure

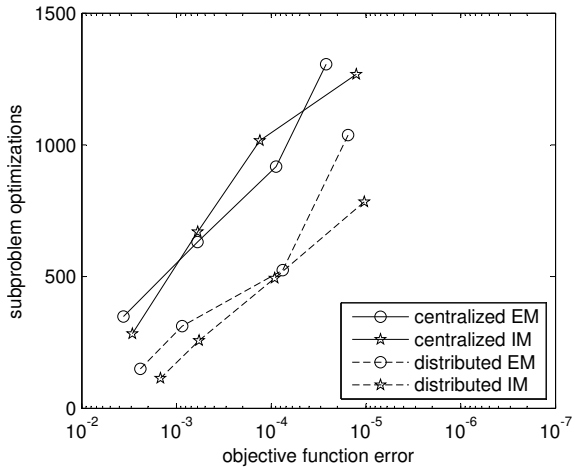

Figure 8: Example 1, Partition 3: Numerical results for centralized (solid lines) and distributed formulation (dashed lines), and exact (EM, ○) and inexact (IM, ⋆) inner loop solution algorithms for different termination tolerances

Costs for Partition 3 are a factor 2-3 higher than for Partition 1, which only has 2 coupling quantities that have to be coordinated between 3 subsystems instead of 8 quantities between 5 subsystems for Partition 3. The differences between Partitions 2 and 3 are however much smaller, even though Partition 2 has only 2 coupling variables instead of 6 for Partition 3. These results indicate that the required solution costs are not only determined by the number of coordinated quantities, but also by some sort of "coupling strength".

4 Portal frame design optimization

The second example is the portal frame design optimization problem originally introduced by Sobieski et al. [3], and used by many other researchers in the context of coordination methods (see, e.g., Refs. [4, 5, 6]). The problem is concerned with finding the cross sectional dimensions of a three beam portal frame, illustrated in Fig. 9(a), which is subjected to a horizontal force and a concentrated moment.

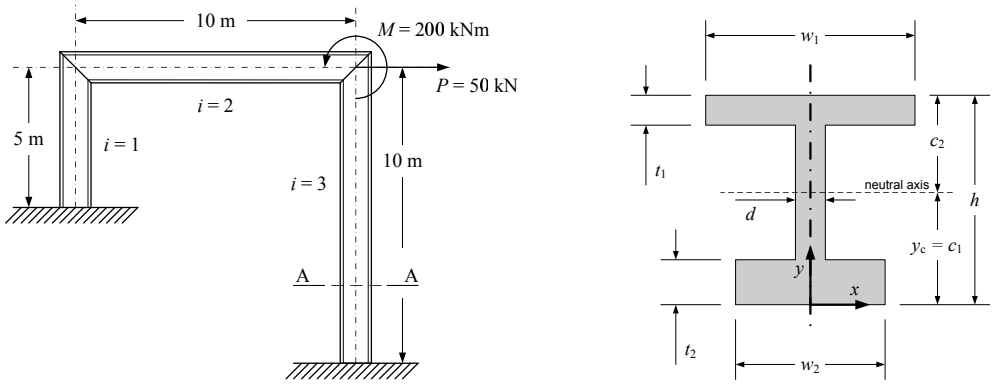

(a) Illustration of the portal frame

(b) Cross-section A—A details. Index 1 refers to the outer faces of the beam.

Figure 9: Portal frame design problem

Although the portal frame problem has been used extensively, no single study reports all implementation details necessary for a reproduction of the presented results. For example, variable bounds are often not reported although they have a large effect on the optimal solution. For the sake of completeness and reproducibility, our implementation details are included in this section, and necessary analysis equations are presented in the Appendix.

4.1 Original all-in-one problem

The optimization problem in this study aims at finding the 18 cross sectional variables ($\mathbf{z} = [\mathbf{z}^{[1]}, \mathbf{z}^{[2]}, \mathbf{z}^{[3]}]$), 6 for each beam ($\mathbf{z}^{[i]} = [h^{[i]}, w_1^{[i]}, w_2^{[i]}, d^{[i]}, t_1^{[i]}, t_2^{[i]}]$, see Fig. 9(b) for definitions), such that the horizontal deflection of the loaded node is minimized. Here, the top-right index refers to one of the three beams. Limits are posed on the total volume of the portal frame (constraint g_1), the rotation of the loaded node (g_2), and normal and shear stresses in all beams (g_3–g_6). Following Ref. [6], geometrical constraints on the beam cross sections (g_7–g_9) are used to prevent slender structures that are likely to buckle.

V_a	$0.30\ \mathrm{m}^3$	allowed volume
θ_a	0.015 rad	allowed rotation of the loaded node
σ_y	$200.0 \cdot 10^6\ \mathrm{N/m}^2$	allowed normal stress
τ_y	$116.0 \cdot 10^6\ \mathrm{N/m}^2$	allowed shear stress

Table 3: Maximally allowed values

The all-in-one portal frame design problem is given by:

$$
\begin{aligned}
\min_{\mathbf{z}} \quad & u_3(\mathbf{z}) \\
\text{subject to} \quad & g_1(\mathbf{z}) = \tfrac{V(\mathbf{z})}{V_a} - 1 \le 0 \\
& g_2(\mathbf{z}) = \tfrac{\theta_3}{\theta_a} - 1 \le 0 \\
& g_{3,i,j,k}(\mathbf{z}) = \tfrac{\sigma_{j,k}^{[i]}}{\sigma_y} - 1 \le 0 && i=1,2,3 \quad j=1,2 \quad k=1,2 \\
& g_{4,i,j,k}(\mathbf{z}) = -\tfrac{\sigma_{j,k}^{[i]}}{\sigma_y} - 1 \le 0 && i=1,2,3 \quad j=1,2 \quad k=1,2 \\
& g_{5,i,j}(\mathbf{z}) = \tfrac{\tau_j^{[i]}}{\tau_y} - 1 \le 0 && i=1,2,3 \quad j=1,2 \\
& g_{6,i,j}(\mathbf{z}) = -\tfrac{\tau_j^{[i]}}{\tau_y} - 1 \le 0 && i=1,2,3 \quad j=1,2 \\
& g_{7,i}(\mathbf{z}^{[i]}) = \tfrac{h^{[i]} - t_1^{[i]} - t_2^{[i]}}{35 d^{[i]}} - 1 \le 0 && i=1,2,3 \\
& g_{8,i,j}(\mathbf{z}^{[i]}) = \tfrac{w_j^{[i]}}{20 t_j^{[i]}} - 1 \le 0 && i=1,2,3 \quad j=1,2 \\
& g_{9,i}(\mathbf{z}^{[i]}) = 1 - \tfrac{5(h^{[i]} - t_1^{[i]} - t_2^{[i]}) d^{[i]}}{A^{[i]}} \le 0 && i=1,2,3 \\
& \mathbf{z}_{\min} \le \mathbf{z} \le \mathbf{z}_{\max}
\end{aligned}
\tag{11}
$$

where the lower and upper bounds on the variables are 10 cm $\le w_1, w_2 \le$ 30 cm, 10 cm $\le h \le$ 50 cm, and 1.0 cm $\le d, t_1, t_2 \le$ 5.0 cm. Constraints g_1 and g_2 pose limits on the total volume of the three beams and the rotation of the loaded node. Constraints g_3 and g_4 limit the normal stress σ in the three beams ($i = 1,2,3$) for both beam ends ($j = 1,2$) at the top and bottom free surfaces ($k = 1,2$). Since the normal stress attains its maximum in one of these locations, constraints g_3 and g_4 effectively assure that the normal stresses are below the allowed value σ_y throughout the whole structure. Similarly, constraints g_5 and g_6 limit the shear stress τ at the neutral axis in the three beams ($i = 1,2,3$) at both ends ($j = 1,2$), which assures that the shear stress does not exceed the allowed value τ_y at any other location. Constraint g_7 limits the aspect ratio of the web of each beam to be smaller than 35, while constraint g_8 limits the aspect ratio of the flanges to be below 20. Constraint g_9 assures that the area of the web is at least 20% of the total cross section area A. The allowed values of constraints g_1 to g_6 are given in Table 3, and the equations required to determine the constraint values are given in the Appendix.

Problem (11) is non-convex and has multiple local minima. To investigate the local solutions, the all-in-one problem (11) was solved with `fmincon` from 1000 different starting points selected randomly within the variable bounds. Optimizer tolerances `TolX`, `TolFun`, and `TolCon`, were set to 10^{-9}, and gradients were computed by the finite difference routine of `fmincon`. For proper scaling, the thickness variables $[d, t_1, t_2]$ are taken in centimeters, and the height/width variables $[h, w_1, w_2]$ are in decimeters. Furthermore, the deflection u_3 (objective function f) is taken in centimeters. Note that the analysis equations of the Appendix require SI units (meters).

Two local solutions are obtained: Solution 1 with a deflection of $\delta^* = 0.92$ cm, beam 2 at the lower bounds, and beams 1 and 3 optimized for minimal deflection; Solution 2 with a deflection of $\delta^* = 2.60$ cm, beam 3 at its lower bounds, and beams 1 and 2 optimized for minimal deflection. Solution 1 was found for the majority of the starting points (96%); only a small number converged to Solution 2 (4%). The mass and maximal deflection constraints are active in all

Local solution 1: $\delta^* = 0.92$ cm

	beam 1	beam 2	beam 3
A	311.7	28.0	116.2
h	50.0	10.0	50.0
w_1	30.0	10.0	22.6
w_2	30.0	10.0	22.6
d	1.50	1.00	1.36
t_1	4.16	1.00	1.13
t_2	4.16	1.00	1.13

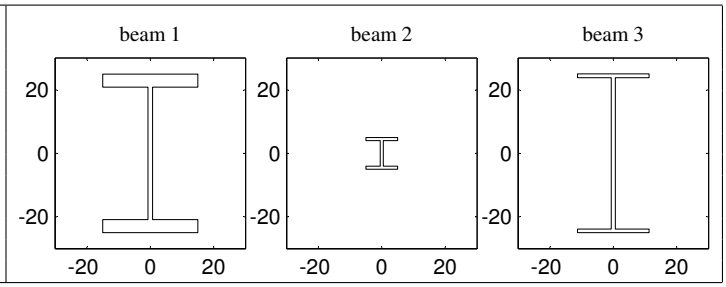

Local solution 2: $\delta^* = 2.60$ cm

	beam 1	beam 2	beam 3
A	242.1	151.0	28.0
h	50.0	50.0	10.0
w_1	30.0	29.6	10.0
w_2	30.0	29.6	10.0
d	1.25	1.34	1.00
t_1	3.12	1.48	1.00
t_2	3.12	1.48	1.00

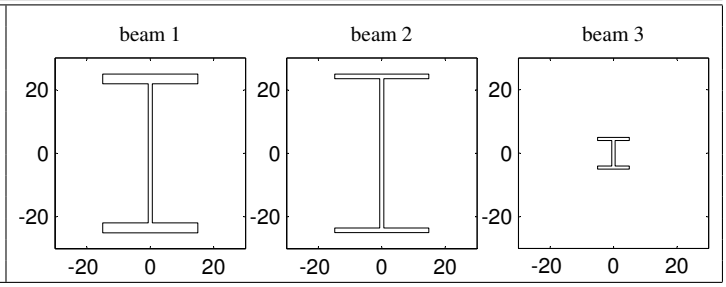

Figure 10: Local solution characteristics (beam dimensions in cm and areas in cm^2)

obtained solutions, together with a number of geometric cross-sectional constraints. The stress constraints are not active in any of the solutions. The local solutions are depicted in Fig. 10.

A qualitative comparison with existing results for the portal frame example shows that the observed trends in the local minima can also be found in the results reported in literature. The results of Refs. [5] and [8] have beam 2 small, while beams 1 and 3 are larger, similar to Solution 1. The results given in Refs. [3], [4], and [6] have beam 3 small and beams 1 and 2 larger, similar to Solution 2.

4.2 Partitioning of the problem

The problem is partitioned in a traditional multi-level fashion (see, e.g. Refs. [3, 7]) by defining three subsystems associated with detailed design of each beam, and a single system-level subsystem concerned with the overall design of the portal frame in terms of the cross sectional areas and moments of inertia $[A^{[1]}, I^{[1]}, A^{[2]}, I^{[2]}, A^{[3]}, I^{[3]}]$. Since the analysis to determine the loads and moments acting on the individual beams depends only on these quantities, the areas and moments are selected to be the system-level design variables. At the beam subsystems, variable copies of the member forces $\mathbf{f}^{[i]},\ i = 1,2,3$ are introduced to determine the stresses in the beams.

Each of the three beam subsystems designs one of the three beams for their detailed cross-sectional dimensions $\mathbf{z}^{[i]},\ i = 1,2,3$. Together with the additionally introduced variables for the member forces $\mathbf{f}^{[i]},\ i = 1,2,3$, this gives for the local variables: $\mathbf{x}^{[i]} = [\mathbf{z}^{[i]}, \mathbf{f}^{[i]}],\ i = 1,2,3$. The local constraints for the beam subsystems are the stress and geometrical constraints $\mathbf{g}_i = [g_{3,i}(\mathbf{x}^{[i]}), \ldots, g_{9,i}(\mathbf{x}^{[i]})]$. The beam subsystems have no local objectives $f_1 = f_2 = f_3 = 0$. For $\mathbf{z}^{[i]}$, the original bounds are used, and the bounds for the member forces are taken such that -10^6 N(m) $\leq \mathbf{f} \leq 10^6$ N(m), where forces are in Newtons and moments in Newton-meters.

The local variables for the system-level are given by $\mathbf{x}_4 = [A^{[1]}, I^{[1]}, A^{[2]}, I^{[2]}, A^{[3]}, I^{[3]}]$, and the objective is $f_4 = f(\mathbf{x}_4) = 0$. The subsystem assures satisfaction of the maximal rotation constraint $\mathbf{g}_4 = [g_2(\mathbf{x}_4)]$, and performs the finite element analysis to determine the member forces $\mathbf{f}^{[i]}_{\text{fem}}(\mathbf{x}_4),\ i = 1,2,3$ required at the beam subsystems. The variable bounds are computed from

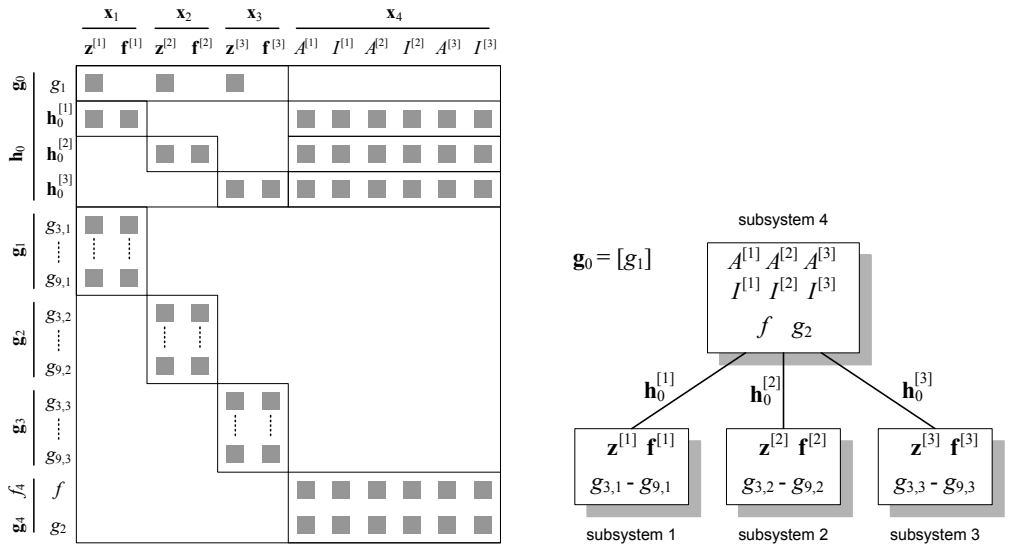

(a) FDT for partitioned portal frame design problem (b) Illustration of partition structure

Figure 11: Portal frame: Partition structure

the bounds for the original variables $\mathbf{z}$, and are set to $2.8 \cdot 10^{-3}$ m^2 $\leq A \leq 5.0 \cdot 10^{-2}$ m^2, and $4.5 \cdot 10^{-6}$ m^4 $\leq I \leq 1.8 \cdot 10^{-3}$ m^4.

The partition has no coupling objective $f_0 = 0$, and the mass constraint $\mathbf{g}_0 = g_1(\mathbf{x}_1, \mathbf{x}_2, \mathbf{x}_3)$ couples the three beam subsystems. The mass constraint could also be included in the system-level problem as a local constraint. Here we treat it as a coupling constraint to add difficulty to the coordination problem.

18 equality constraints $\mathbf{h}_\mathrm{f} = [\mathbf{h}_\mathrm{f}^{[1]}, \mathbf{h}_\mathrm{f}^{[2]}, \mathbf{h}_\mathrm{f}^{[3]}] = \mathbf{0}$ are introduced to couple the member force variables $\mathbf{f}^{[i]}$ of each beam subsystem to the values $\mathbf{f}_\mathrm{fem}^{[i]}(\mathbf{x}_4)$ computed at the system level, where

$$\mathbf{h}_\mathrm{f}^{[i]} = \mathbf{f}^{[i]} - \mathbf{f}_\mathrm{fem}^{[i]}(\mathbf{x}_4) \tag{12}$$

6 equality constraints $\mathbf{h}_\mathrm{a} = [\mathbf{h}_\mathrm{a}^{[1]}, \mathbf{h}_\mathrm{a}^{[2]}, \mathbf{h}_\mathrm{a}^{[3]}] = \mathbf{0}$ are introduced to link the areas and the moments of inertia $A^{[i]}, I^{[i]}$ used at the system-level problem to the values associated with the detailed cross-section dimensions $A_\mathrm{beam}^{[i]}(\mathbf{x}_i)$, $I_\mathrm{beam}^{[i]}(\mathbf{x}_i)$, where

$$\mathbf{h}_\mathrm{a}^{[i]} = \begin{bmatrix} A^{[i]} - A_\mathrm{beam}^{[i]}(\mathbf{x}_i) \\ I^{[i]} - I_\mathrm{beam}^{[i]}(\mathbf{x}_i) \end{bmatrix} \tag{13}$$

where the area $A_\mathrm{beam}^{[i]}(\mathbf{x}_i)$ and moment of inertia $I_\mathrm{beam}^{[i]}(\mathbf{x}_i)$ of beam i are given by Eqs. (14)–(15).

These introduced constraints couple the beam subsystems to the system level, and are therefore the coupling equality constraints of the problem: $\mathbf{h}_0(\mathbf{x}_1, \mathbf{x}_2, \mathbf{x}_3, \mathbf{x}_4) = [\mathbf{h}_0^{[1]}, \mathbf{h}_0^{[2]}, \mathbf{h}_0^{[3]}]$ with $\mathbf{h}_0^{[i]}(\mathbf{x}_i, \mathbf{x}_4) = [\mathbf{h}_\mathrm{f}^{[i]}, \mathbf{h}_\mathrm{a}^{[i]}]$. The partition structure is depicted in Fig. 11.

Algorithm	group 1 $\delta^* = 0.92$	group 2 $\delta^* = 2.60$
`fmincon`*	96%	4%
exact EM	100%	0%
inexact IM	100%	0%

*all-in-one formulation

Table 4: Distribution of local solutions for different coordination algorithms

4.3 Numerical results

The partitioned problem is decomposed in a distributed formulation that overlaps the partition structure as depicted in Fig. 11(b). Similar to the all-in-one experiments, the decomposed problem is solved from 1000 different starting points selected randomly within the variable bounds. Both an exact (EM) and an inexact (IM) method of multipliers are used to solve the decomposed problem, both with an outer loop termination tolerance of 10^{-3}. The remaining algorithmic settings are chosen as for the geometric programming problem experiments of Section 3.1. Note that we use an SQP algorithm for solution of the subproblems, which does not guarantee that globally optimal subproblem solutions are attained.

For scaling, $[d,t_1,t_2]$ are again taken in centimeters, $[h,w_1,w_2]$ are in decimeters, and the objective u_3 in centimeters. Areas A are in 10^{-2} m^2, I in 10^{-4} m^4, and forces $\mathbf{f}$ in 10^4 N(m). Furthermore, constraints $\mathbf{h}_0$ use scaled units instead of SI units.

Both the exact and the inexact method converge to Solution 1 of the original problem for all starting points (see Table 4), which shows that no additional local minima are introduced by decomposing the problem. Solution 2 was not obtained in any of the experiments. For this example problem, the decomposition-based approach eliminated convergence to a poor local solution, even though all subproblem optimizations are performed with a local optimization technique. This may be due to gradually enforcing coupling and consistency constraints through the augmented Lagrangian penalty function. For this example, the coordination algorithm shows a preference for the better of the two local solutions. For the general case however, whether and which solutions are eliminated depends on both the problem, and the initial design and parameter settings.

The exact algorithm EM required an average of 261 subproblem optimizations to converge, with a solution error of $e = 1.1 \cdot 10^{-4}$. The inexact IM required only 200 subproblem optimizations, and an average error of $e = 1.7 \cdot 10^{-4}$. Again, the inexact inner loop reduces computational cost by terminating the inner loop early in the first 10 iterations.

Note that the solution costs for the portal frame example are about 50% lower than the costs observed for Partition 3 of the previous example for a similar error. Although the portal frame partition has a larger number of coupling quantities (25 coupling constraints between 4 subsystems), it requires less solution effort than Partition 3 which has only 9 coupling quantities between 5 subsystems. This confirms our findings discussed for the previous example in Section 3 that coordination cost are not only determined by the number of coordinated quantities, but also by some sort of "coupling strength".

5 Conceptual design of a supersonic business jet

A conceptual supersonic business jet design problem serves as the third example. This example is taken from Ref. [9], and modified versions have been used to demonstrate the use of other coordination algorithms (see, e.g., [10]).

5.1 Original all-in-one problem

The optimization problem is concerned with maximizing the range of the aircraft while considering structures, aerodynamics, propulsion, and range subsystems. The four subsystems and their data dependencies are displayed in Fig. 12. In this figure, **z** variables (8 in total) are shared by all subsystems, **x** variables (23 in total) are local to a single discipline, and the behavior variables communicated between the subsystems are denoted by **y** variables (9 in total), and reflect analysis input and output data dependencies. Table 5 gives a brief description of the variables. The problem has a total of 40 design variables, and 45 design constraints. The reader is referred to Ref. [9] for a full description of the problem.

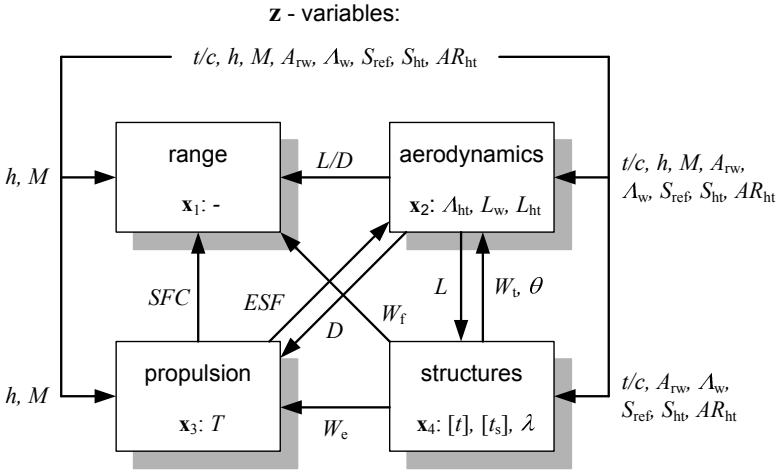

Figure 12: Example 3: Data dependencies for business jet problem

Results from the all-in-one implementation of the problem[2] with IDF (individual discipline feasible, see Ref. [12]) of the problem indicate that multiple local minima exist. A total of 15 different solutions was observed after solving the problem 1000 times from different starting point selected randomly within the variable bounds. Only 455 runs were reported (by NPSOL) to have converged to a solution. Optimized range values varied from 1869 to 3850 nautical miles, and the majority of the converged runs (97%) have a optimal range larger than 3650 nautical miles. 65% terminated at a range value of 3694 nautical miles. The observed optimal designs show many similarities in the **z** and **x** design variables. The main differences between the solutions arise for the thickness to chord ratio (t/c), the wing sweep angle (Λ_w), and the wing thicknesses ($[t]$ and $[t_s]$). Optimal values for the behavioral variables **y** are also non-common, except the specific fuel consumption (SFC). Details on the optimal values are given in Table 5.

[2] NPSOL solver of Tomlab [11] was used with default settings, and gradients were computed by the built-in finite difference routine.

z variables		optimal	**x** variables		optimal	**y** variables		optimal
t/c	thickness/chord	nc	Λ_{ht}	tail sweep	70°	L	total lift	nc
h	altitude	60000 ft	L_w	wing lift	0.01 %MAC	W_e	engine weight	nc
M	Mach number	1.5	L_{ht}	tail lift	3.5 %MAC	W_t	total weight	nc
AR_w	wing aspect ratio	2.5	T	throttle	0.17	θ	wing twist	nc
Λ_w	wing sweep angle	nc	$[t]$	9 thicknesses	nc	ESF	engine scaling factor	nc
S_{ref}	wing surf. area	800 ft^2	$[t_s]$	9 thicknesses	nc	D	total drag	nc
S_{ht}	tail surf. area	149 ft^2	λ	taper ratio	0.1	W_f	fuel weight	nc
AR_{ht}	tail aspect ratio	2.5				L/D	lift/drag	nc
						SFC	spec. fuel cons.	1.0

Table 5: Example 3: Variable description and common optimal values (nc = non-common optimal value)

Of all the obtained solutions, not a single one satisfies the Karush-Kuhn-Tucker (KKT) conditions for optimality. At every solution, the gradient of the Lagrangian is non-zero, possibly caused by a discontinuity or non-smoothness in one of the subsystems. Failure to meet the KKT conditions at solutions may cause difficulties for the coordination method since the convergence proofs assume that the KKT conditions are satisfied at solutions to the all-in-one problem. For many existing coordination methods, the use of response surface methods (RSM) has been proposed to avoid the difficulties associated with non-smoothness of functions (see, e.g., Refs. [6, 10]). Although such a smoothing approach could also be used for the augmented Lagrangian coordination method, we are here interested in the performance of the method in conditions that are outside the assumptions of the theory. Therefore, we investigate the performance of the coordination method when directly applied to the non-smooth problem.

5.2 Partitioning of the problem

Two partitions of the problem are used: a traditional, multi-disciplinary partition with a central coordinator that includes the objective, and a distributed partition in which the objective is used as a coupling variable. In the first partition, the range subsystem is superimposed over the remaining three disciplines, and acts as a central coordinator (Fig. 13). For this choice, the structures, aerodynamics, and propulsion subsystems are decoupled and can be solved in parallel. The coupling variables are the system variables **z**, and the behavior variables **y**. The second partition takes the range equation as a coupling objective, which eliminates the range subproblem from the partition altogether (see Fig. 14). Due to the coupling objective, the subsystems cannot be solved in parallel, but have to be solved sequentially. Coupling variables between the remaining subsystems are coordinated directly between the subproblems. Furthermore, three behavioral variables, required as inputs for the range subsystem, become local to a subsystem (i.e., L/D for aerodynamics, SFC for propulsion, and W_f for structures). Note that the elimination of the range subsystem requires the range computation to be performed at *all* subsystems. For this example, such an approach does not pose difficulties since the range computation is performed through the analytical Breguet range equation.

By using the range equation as a coupling objective, one subsystem could be removed, and the number of coupling quantities was reduced from 31 in the traditional partition to 15 in the new partition. This reduction in partition complexity is expected to have a substantial effect on the required coordination costs.

5.3 Numerical results

Both partitions are solved with an exact inner loop (EM) and an inexact inner loop (IM). Outer loop termination tolerances for all experiments are set to $\varepsilon = 10^{-3}$, and the remaining algorithmic settings are chosen as for the geometric programming problem experiments of Section 3.1. Five different starting points, distributed randomly within the variable bounds, are used for each

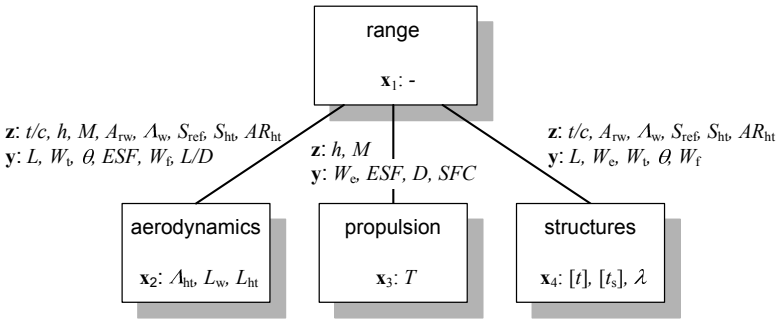

Figure 13: Example 3: Traditional centralized partition

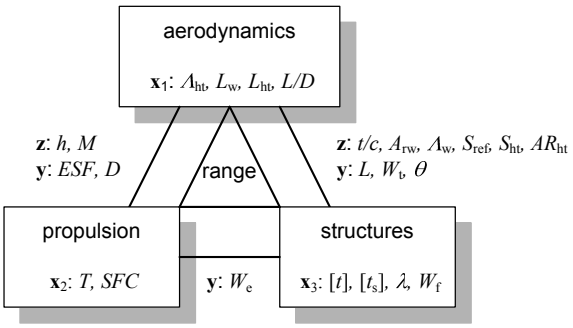

Figure 14: Example 3: Partition with range equation as coupling objective

experiment.

Since the all-in-one problem showed convergence difficulties for some starting points, similar behavior is expected for the subproblems (and observed in practice). Experiments indicate that communicating non-converged inaccurate solutions results in convergence difficulties of the coordination algorithm. To avoid difficulties, only converged solutions are passed. Non-converged subproblem solutions are restarted at a perturbed starting point until a converged solution is obtained. With this approach, the coordination method will not be prematurely terminated by unsuccessful subproblem optimizations.

The majority of the experiments for both partitions and coordination strategies (EM and IM) converged to one of the all-in-one solutions even though these points are not KKT points of the original problem. For the first partition, two out of five runs for both EM and IM converged to a non-optimal solution with a range of around 3300 nautical miles. Although non-optimal, these final designs are consistent and feasible. The non-optimal designs for the first partition typically have a smaller tail (110–120 ft^2) with a higher aspect ratio (≈ 5), a larger mach number (≈ 1.8), and a larger throttle (≈ 0.25). The remaining common design variables obtained with the coordination algorithm are equal to the optimal values of all-in-one implementation. For the second partition, all experiments converged to an all-in-one solution.

Table 6 shows the total number of subproblem optimizations required for convergence for both partitions. As expected, a large difference in solution cost is observed between the two partitions. The traditional partition requires almost five times more subproblem optimizations than the second partition with the coupling objective. Even if parallelism would be taken into account (at most a factor 3 could be gained), the reduction in coupling quantities through the use of the coupling objective is successful in reducing the solutions costs for this example.

		optimal	cost
partition 1	exact	60 %	2427
	inexact	60 %	2342
partition 2	exact	100 %	500
	inexact	100 %	483

Table 6: Example 3 coordination results summary: Percentage of solutions that converged to an optimal all-in-one solution and average number of subproblem optimizations required for convergence.

When comparing the results from the exact and inexact inner loops, only a small difference is observed. Terminating the inner loop early for the first 10 iterations appears not to yield a computational advantage for this example.

The above results show that the coordination method is able to find consistent and feasible solutions for this example that does not satisfy all assumptions of the convergence proof. Furthermore, the performance of the coordination method is not heavily affected by the non-smoothness of the problem.

6 Conclusions and discussion

This paper showed that the augmented Lagrangian coordination method is a flexible and effective coordination method that can be used to solve MDO problems in a traditional centralized fashion, but also in a distributed fashion. The method was demonstrated to provide a large degree of flexibility in formulating the decomposed problem. Numerical experiments with two non-convex example problems demonstrated the method's effectiveness in finding solutions to the original non-decomposed. Furthermore, the method was found to be robust and provided accurate solutions for the business jet example in which not all assumptions of the convergence proof are satisfied.

Results indicate that coordination costs depend heavily on the partition of the problem. We expect that costs can be reduced significantly by (model-based) selection of a "smart" partition with low coupling strength. Such an approach would require two ingredients: A method for quantifying coupling strength, and an algorithm to find a partition with minimal coupling strength. Developments in the fields of coupling strength quantification (see, e.g., Refs. [15, 16, 17, 18]) and model-based partitioning (see, e.g., Refs. [19, 20, 21]) are expected to be of great value in this context.

A suggestion for enhancement of our method would be to develop an alternative, more efficient inner loop algorithm. The currently used block coordinate descent (BCD) method operates in a Gauss-Seidel fashion, and its convergence rate is at best linear. From experiments we observe that this linear convergence rate limits the efficiency of the coordination method. To illustrate this observation, consider Figure 15, which depicts the convergence history of the objective for an experiment of the business jet example. The displayed convergence behavior is typical for all examples in this paper. The figure shows that the inner loop becomes very slow after a number of outer loop penalty updates. For this example, only little progress is made in the final 200 subproblem optimizations, where an inner loop can require up to 100 iterations. This behavior is caused by the increased coupling between the subproblems through the penalty terms, which becomes larger as penalty weights are increased, and was also observed for other coordination methods (see Refs. [13, 14]). Possible enhancements for the inner loop could use separable approximations of the penalty terms, similar to the methods of Refs. [22] and [23], a quadratically

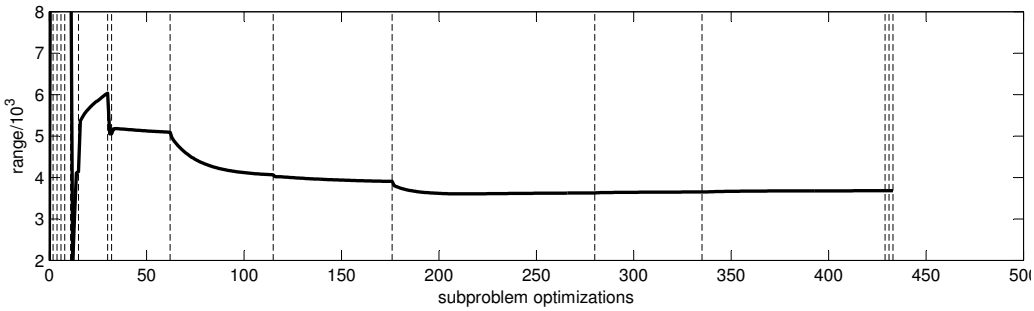

Figure 15: Example 3: Sample of objective function convergence history for partition 2 and inexact method of multipliers (vertical lines indicate outer loop penalty parameter updates)

convergent inner loop strategy as used in Ref. [24], or a truncated inner loop similar to the alternating direction algorithm of Ref. [14].

Bibliography

[1] Tosserams S, Etman LFP, Rooda JE. Generalization of Analytical Target Cascading for distributed optimal design: Part I formulation. *International Journal for Numerical Methods in Engineering*, 2007; **?**(?):?–?.

[2] Mathworks. *Matlab User Guide*. www.mathworks.com; date of reference 5 January 2007.

[3] Sobieszczanski-Sobieski J, James BB, Dovi AR. Structural optimization by multilevel decomposition. *AIAA Journal*, 1985; **23**:1775–1782.

[4] Vanderplaats GN, Yang YJ, Kim DS. Sequential linearization method for multilevel optimization. *AIAA Journal*, 1989; **28**(2):290–295.

[5] Arslan MA, Hajela P. Counterpropagation neural networks in decomposition based optimal design. *Computers and Structures*, 1997; **65**(5):641–650.

[6] Liu B, Haftka RT, Watson LT. Global-local structural optimization using response surfaces of local optimization margins. *Structural and Multidisciplinary Optimization*, 2004; **27**(5):352Ű-359.

[7] Haftka RT, Gürdal Z. *Elements of Structural Optimization*, (3rd ed.). Kluwer Publishers, 1992.

[8] Schutte JF, Haftka RT, Watson LT. Decomposition and two-level optimization of structures with discrete sizing variables. In: proceedings of the 45th AIAA/ASME/ASCE-AHS/ASC Structures, Structural Dynamics, and Materials Conference, Palm Springs, CA, April 2004. AIAA paper 2004-1541.

[9] Agte JS, Sobieszczanski-Sobieski J, Sandusky RR Jr. Superosnic business jet design through bi-level integrated system synthesis. In: proceedings of the World Aviation Conference, San Fransisco, CA, October 1999. SAE paper 1999-01-5622.

[10] Sobieszczanski-Sobieski J, Altus TD, Phillips M, Sandusky Jr RR. Bilevel Integrated System Synthesis for concurrent and distributed processing. *AIAA Journal*, 2000; **41**(10):1996–2003.

[11] Holmström K, Göran AO, Edvall MM. *User's Guide for Tomlab*. Tomlab Optimization Inc., 2006. www.tomopt.com.

[12] Cramer EJ, Dennis JE, Frank PD, Lewis RM, Shubin GR. Problem formulation for multidisciplinary optimization. *SIAM Journal of Optimization*, 1994; **4**(4):754–776.

[13] Tzevelekos N, Kokkolaras M, Papalambros PY, Hulshof MF, Etman LFP, Rooda JE. An empirical local convergence study of alternative coordination schemes in analytical target cascading. In: proceedings of the 5th World Congress on Structural and Multidisciplinary Optimization, Lido di Jesolo, Venice, Italy, May 2003.

[14] Tosserams S, Etman LFP, Rooda JE. An augmented Lagrangian decomposition method for quasi-separable problems in MDO. *Structural and Multidisciplinary Optimization*, 2007; DOI 10.1007/s00158-006-0077-z. To appear.

[15] Sobieszczanski-Sobieski J. Sensitivity of complex, internally coupled systems. *AIAA Journal*, 1990; **28**(1):153–160.

[16] Sobieszczanski-Sobieski J, Agte JS, Sandusky Jr. RR. Bilevel Integrated System Synthesis. *AIAA Journal*, 2000; **38**(1):164–172.

[17] Alyaqout SF, Papalambros PY, Ulsoy AG. Quantification and use of system coupling in decomposed design optimization problems. In: proceedings of the ASME International Mechanical Engineering Congress and Exposition, Orlando, Florida, November 2005.

[18] Allison JT, Kokkolaras M, Papalambros PY. Analysis of single-level formulations for complex system design. *Journal of Mechanical Design*, 2006; accepted

[19] Michelena NF, Papalambros PY. A hypergraph framework for optimal model-based decomposition of design problems. *Computational Opimization and Applications*, 1997; **8**(2):173–196.

[20] Ferris MC, Horn JD. Partitioning mathematical programs for parallel solution. *Computational Opimization and Applications*, 1998; **8**(2):173–196.

[21] Li S, Chen L. Model-based decomposition using non-binary dependency analysis and heuristic partitioning analysis. In: proceedings of the ASME International Design Engineering Technical Conferences & Computers and Information in Engineering Conference, Philadelphia, Pennsylvania, September 2006.

[22] Ruszczynski A. On convergence of an augmented Lagrangian decomposition method for sparse convex optimization. *Mathematics of Operations Research*, 1995; **20**: 634–656

[23] Censor Y, Zenios SA. *Parallel Optimization: Theory, Algorithms, and Applications*. Oxford University Press, 1997.

[24] DeMiguel AV, Murray W. A local convergence analysis of bilevel decomposition algorithms. *Optimization and Engineering*, 2006; **7**:99–133.

Appendix:
Analysis equations for portal frame example

Cross-Section Properties

The area $A^{[i]}$ and moment of inertia $I^{[i]}$ of beam i are given by (indices i dropped for brevity of notation):

$$A = w_1 t_1 + (h - t_1 - t_2)d + w_2 t_2 \tag{14}$$

$$I = \frac{w_1 (t_1)^3}{12} + w_1 t_1 (y_c - (h - \frac{1}{2} t_1))^2 + \frac{d(h - t_1 - t_2)^3}{12} + d(h - t_1 - t_2)(y_c - \frac{1}{2} h)^2 + \frac{w_2 (t_2)^3}{12} + w_2 t_2 (y_c - \frac{1}{2} t_2)^2 \tag{15}$$

where the centroid y_c is given by:

$$y_c = \frac{w_1 t_1 (h - \frac{1}{2} t_1) + \frac{1}{2}(h - t_1 - t_2) d h + \frac{1}{2} w_2 (t_2)^2}{w_1 t_1 + d(h - t_1 - t_2) + w_2 t_2} \tag{16}$$

The first moment of area Q of the material above the neutral axis for a beam, relevant in computing the shear stress, is given by:

$$Q = w_1 t_1 (h - y_c - \frac{1}{2} t_1) + \frac{1}{2} d (h - y_c - t_1)^2 \tag{17}$$

The free surface distances c_1 and c_2, required for determining the maximal bending stress, are given by:

$$c_1 = h - y_c \qquad\qquad c_2 = y_c \tag{18}$$

at the faces of flanges 1 (outer) and 2 (inner), respectively.

Unknown displacements and reaction forces

To determine the stresses in the frame, first the forces and moments acting on the individual beams have to be computed. To this end, we use a finite element analysis that consists of three plane bending elements, each associated with one I beam of the frame. Each end $j = 1,2$ of a beam element is subjected to an axial force N_j, a shear force V_j, and a bending moment M_j. The positive directions in each beam are defined as illustrated in Fig. 16.

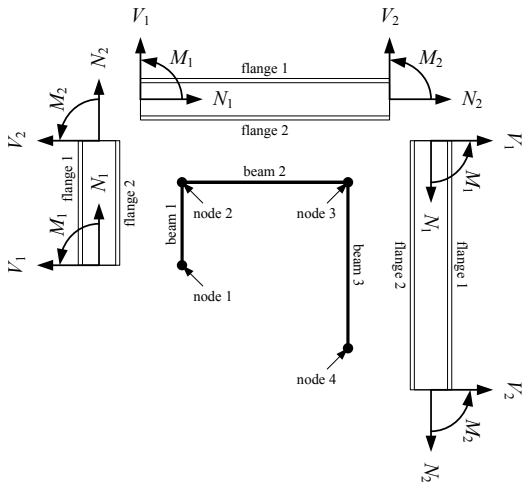

Figure 16: Free body diagrams of portal frame beams

The vector of member forces $\mathbf{f}$ is given by: $\mathbf{f} = [N_1, V_1, M_1, N_2, V_2, M_2]^T$, and the vector of local member node displacements $\mathbf{u}$ is given by $\mathbf{u} = [u_1, v_1, \theta_1, u_2, v_2, \theta_2]^T$, where u_j, v_j, and θ_j are the axial and perpendicular displacements, and the rotation of beam end j, respectively. The positive directions of the displacements coincide with the positive directions of the member forces.

First, we consider the boundary conditions of the construction. From the boundary conditions we know that nodes 1 and 4 are fixed $[u_1, v_1, \theta_1] = [u_4, v_4, \theta_4] = [0,0,0]$, and the reaction forces at nodes 2 and 3 are known: $[X_2, Y_2, Z_2] = [0,0,0]$ and $[X_3, Y_3, Z_3] = [50 \cdot 10^3, 0, 200 \cdot 10^3]$ (see Fig. 16 for the definition of the node numbers). The remaining displacements $[u_2, v_2, \theta_2]$ and $[u_3, v_3, \theta_3]$, and reaction forces $[X_1, Y_1, Z_1]$ and $[X_4, Y_4, Z_4]$ are unknown.

To compute these unknowns, the displacement and force vectors are split up into two parts: a known part (boundary conditions) and an unknown part (free nodes), such that $\mathbf{u}_{\text{ass}} = [\mathbf{u}_{\text{free}}^T, \mathbf{u}_{\text{bc}}^T]^T$ and $\mathbf{f}_{\text{ass}} = [\mathbf{f}_{\text{bc}}^T, \mathbf{f}_{\text{free}}^T]^T$, where $\mathbf{u}_{\text{free}} = [u_2, v_2, \theta_2, u_3, v_3, \theta_3]^T$, $\mathbf{u}_{\text{bc}} = [u_1, v_1, \theta_1, u_4, v_4, \theta_4] = [0,0,0,0,0,0]^T$, $\mathbf{f}_{\text{bc}} = [X_2, Y_2, Z_2, X_3, Y_3, Z_3] = [0,0,0,50 \cdot 10^3, 0, 200 \cdot 10^3,]^T$, and $\mathbf{f}_{\text{free}} = [X_1, Y_1, Z_1, X_4, Y_4, Z_4]^T$.

Under these conventions, the unknowns can be computed by the system of equations $\mathbf{K}_{\text{ass}}\mathbf{u}_{\text{ass}} = \mathbf{f}_{\text{ass}}$, which is given by:

$$\begin{bmatrix} \mathbf{K}_{11} & \mathbf{K}_{12} \\ \mathbf{K}_{12}^T & \mathbf{K}_{22} \end{bmatrix} \begin{bmatrix} \mathbf{u}_{\text{free}} \\ \mathbf{u}_{\text{bc}} \end{bmatrix} = \begin{bmatrix} \mathbf{f}_{\text{bc}} \\ \mathbf{f}_{\text{free}} \end{bmatrix} \tag{19}$$

where $\mathbf{K}_{11}$, $\mathbf{K}_{12}$, and $\mathbf{K}_{22}$ are 6×6 submatrices of the assembled stiffness matrix $\mathbf{K}_{\text{ass}}$.

From this system, and because $\mathbf{u}_{\text{bc}} = 0$, the free displacements are given by:

$$\mathbf{u}_{\text{free}} = \mathbf{K}_{11}^{-1}(\mathbf{f}_{\text{bc}} - \mathbf{K}_{12}\mathbf{u}_{\text{bc}}) = \mathbf{K}_{11}^{-1}\mathbf{f}_{\text{bc}} \tag{20}$$

The unknown reaction forces $\mathbf{f}_{\text{free}} = [X_1, Y_1, Z_1, X_4, Y_4, Z_4]^T$ are given by:

$$\mathbf{f}_{\text{free}} = \mathbf{K}_{12}^T\mathbf{u}_{\text{free}} + \mathbf{K}_{22}\mathbf{u}_{\text{bc}} = \mathbf{K}_{12}^T\mathbf{K}_{11}^{-1}\mathbf{f}_{\text{bc}} \tag{21}$$

Assembled stiffness matrix

The assembled stiffness $\mathbf{K}_{\text{ass}}$ matrix is constructed from the local stiffness matrices of each beam. The local stiffness matrix that relates the member forces to the member displacements (in the local coordinate system) through $\mathbf{f} = \mathbf{K}_{\text{local}}\mathbf{u}$ is given by (beam indices dropped for brevity of notation):

$$\mathbf{K}_{\text{local}} = \begin{bmatrix} \frac{EA}{L} & 0 & 0 & -\frac{EA}{L} & 0 & 0 \\ 0 & \frac{12EI}{L^3} & \frac{6EI}{L^2} & 0 & -\frac{12EI}{L^3} & \frac{6EI}{L^2} \\ 0 & \frac{6EI}{L^2} & \frac{4EI}{L} & 0 & -\frac{6EI}{L^2} & \frac{2EI}{L} \\ -\frac{EA}{L} & 0 & 0 & \frac{EA}{L} & 0 & 0 \\ 0 & -\frac{12EI}{L^3} & -\frac{6EI}{L^2} & 0 & \frac{12EI}{L^3} & -\frac{6EI}{L^2} \\ 0 & \frac{6EI}{L^2} & \frac{2EI}{L} & 0 & -\frac{6EI}{L^2} & \frac{4EI}{L} \end{bmatrix} \tag{22}$$

To create the assembled stiffness matrix, first the element stiffness matrices have to be rotated from the local to the global coordinate system. To this end, a rotation matrix $\mathbf{R} = \mathbf{R}(\alpha)$ is used such that $\mathbf{K} = (\mathbf{R})^T\mathbf{K}_{\text{local}}\mathbf{R}$, where the matrix $\mathbf{R} = \mathbf{R}(\alpha)$ is given by:

$$\mathbf{R} = \mathbf{R}(\alpha) = \begin{bmatrix} \cos(\alpha) & \sin(\alpha) & 0 & 0 & 0 & 0 \\ -\sin(\alpha) & \cos(\alpha) & 0 & 0 & 0 & 0 \\ 0 & 0 & 1 & 0 & 0 & 0 \\ 0 & 0 & 0 & \cos(\alpha) & \sin(\alpha) & 0 \\ 0 & 0 & 0 & -\sin(\alpha) & \cos(\alpha) & 0 \\ 0 & 0 & 0 & 0 & 0 & 1 \end{bmatrix} \tag{23}$$

The rotation angles α for the three beams are: $\alpha^{[1]} = \pi/2$, $\alpha^{[2]} = 0$, and $\alpha^{[3]} = -\pi/2$.

To determine the assembled stiffness matrix $\mathbf{K}_{\text{ass}}$ for the whole structure, the local nodes are mapped to the global nodes, and the rotated local stiffness matrices are inserted at the appropriate places of the assembled stiffness matrix $\mathbf{K}_{\text{ass}}$. To this end, a projection matrix $\mathbf{P}^{[i]}$ for beam i can be defined such that:

$$\mathbf{K}_{\text{ass}} = \sum_{i=1}^{3} (\mathbf{P}^{[i]})^T \mathbf{K}^{[i]} \mathbf{P}^{[i]} \tag{24}$$

For beams 1, 2, and 3 the projection matrices are given by:

$$\mathbf{P}^{[1]} = \begin{bmatrix} \mathbf{0} & \mathbf{0} & \mathbf{I} & \mathbf{0} \\ \mathbf{I} & \mathbf{0} & \mathbf{0} & \mathbf{0} \end{bmatrix} \qquad \mathbf{P}^{[2]} = \begin{bmatrix} \mathbf{I} & \mathbf{0} & \mathbf{0} & \mathbf{0} \\ \mathbf{0} & \mathbf{I} & \mathbf{0} & \mathbf{0} \end{bmatrix} \qquad \mathbf{P}^{[3]} = \begin{bmatrix} \mathbf{0} & \mathbf{I} & \mathbf{0} & \mathbf{0} \\ \mathbf{0} & \mathbf{0} & \mathbf{0} & \mathbf{I} \end{bmatrix} \tag{25}$$

with $\mathbf{I}$ the 3×3 identity matrix and $\mathbf{0}$ a 3×3 zero matrix.

Computation of Stresses

The nodal forces $\mathbf{f}^{[i]}$ in beam i, required for computing the stresses, are given by (indices i dropped again):

$$\mathbf{f} = [N_1, V_1, M_1, N_2, V_2, M_2]^T = \mathbf{K}_{\text{local}} \mathbf{u} = \mathbf{K}_{\text{local}} \mathbf{R} \mathbf{P} \mathbf{u}_{\text{ass}} \tag{26}$$

The axial stress σ_{a} is constant throughout a beam and is given by:

$$\sigma_{\text{a}} = \frac{N_2 - N_1}{A} \tag{27}$$

The bending stresses $\sigma_{\text{b},j,k}$ at end $j = 1,2$ in the top ($k = 1$) and bottom ($k = 2$) flanges of beam i, respectively, are given by:

$$\sigma_{\text{b},1,1} = \frac{c_1 M_1}{I} \qquad \sigma_{\text{b},1,2} = -\frac{c_2 M_1}{I} \qquad \sigma_{\text{b},2,1} = -\frac{c_1 M_2}{I} \qquad \sigma_{\text{b},2,2} = \frac{c_2 M_2}{I} \tag{28}$$

The four normal stresses $\sigma_{j,k}$ at flanges $k = 1,2$ of beam ends $j = 1,2$ are given by:

$$\sigma_{j,k} = \sigma_{\text{a}} + \sigma_{\text{b},j,k} \qquad j = 1,2 \qquad k = 1,2 \tag{29}$$

The shear stresses τ_j at the neutral axis at the beams ends $j = 1,2$ are given by:

$$\tau_j = \frac{V_j Q}{Id} \qquad j = 1,2 \tag{30}$$